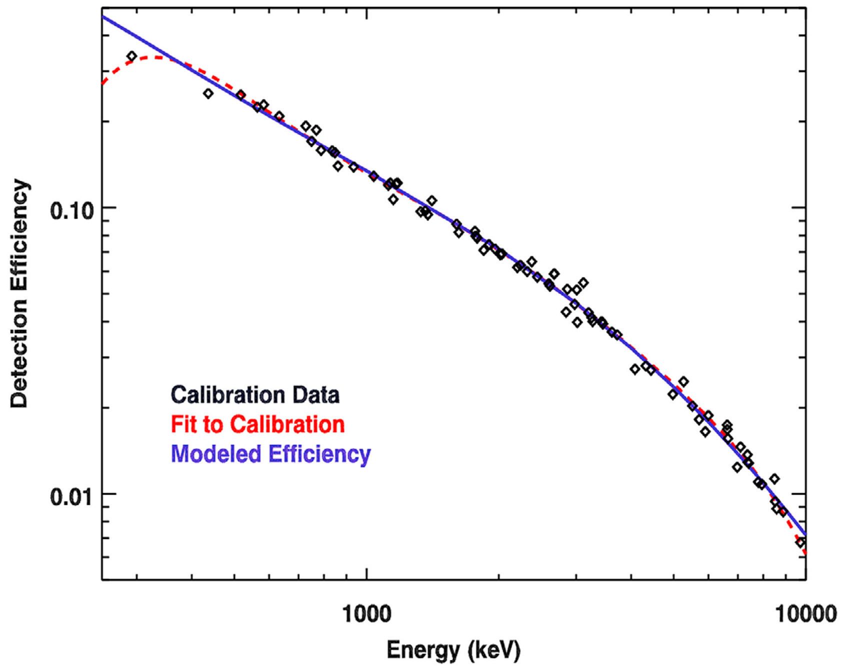

Figure A2. A comparison between the $\theta_D = 0°$ ground calibration measurements of gamma-ray photopeak detection efficiency and the Geant4-simulated detector response. The close agreement between these values, as well as ground calibration data taken at θ_D = 22.5, 45, and 67.5° for a wide range of ϕ_D values, validated the simulations, which were extended to create maps of the efficiency for arbitrary energy and incidence angle (e.g., Figure A4).

calibration measurements and the sixth-degree polynomial fit of ln(ε) versus ln(E_γ) that describes energy-dependent detection efficiency at this orientation, where ε is the intrinsic detection efficiency and E_γ is the gamma-ray energy. Despite the large number of ground calibration measurements that were taken, they cover only a limited range of the total relevant gamma-ray incidence angles, necessitating the use of radiation transport modeling to create an efficiency map for the GRS at arbitrary incident energies and angles.

A3. Modeled Response

[51] The radiation transport modeling code Geant4 [*Agostinelli et al.*, 2003] was used to model the response of the GRS. Geant4 has a heritage of space-based applications; for example, it was applied toward modeling the efficiency of the Gamma-ray Spectrometer on the SELENE lunar mission of the Japan Aerospace Exploration Agency [*Kobayashi et al.*, 2010]. A custom Geant4 application was created to model the efficiency of the MESSENGER GRS, using original computer-aided design (CAD) drawings to reproduce the dimensions and material compositions of the instrument. The simulations were benchmarked with the ground-calibration measurements at hundreds of different gamma-ray energies and incident angles. The results of a subset of these simulations are shown in Figure A2. A 4% reduction in the dimensions of the HPGe crystal was required to match the $\theta_D = 0°$ ground calibration measurements, probably originating from the fact that the active volume of the crystal was slightly smaller than its total volume. Following this correction, the simulations were found to agree with the ground calibration measurements to within 5% for all $\theta_D > 0°$ measurements without further modification to the detector geometry. This agreement facilitated the expansion of the simulations to model the detector response for arbitrary gamma-ray energies and incident angles, including the effects of gamma-ray attenuation by GRS-surrounding spacecraft components.

[52] The FASTRAD toolkit [e.g., *Pourrouquet et al.*, 2011] was used to import the CAD geometries of the spacecraft components and instruments surrounding the GRS (Figure A3) into the Geant4 application to reproduce the upper third of the spacecraft. With this model, the efficiency of the GRS was characterized for incident angles ranging over $0° < \theta_D < 130°$ in a $2° \times 2°$ grid in θ_D and φ_D space. Figure A4 shows the resulting efficiency map for the 1461-keV gamma ray. Similar maps were created for all of the gamma rays of interest for this study. The attenuation of incident gamma rays is evident in this efficiency map as a reduction in the detection efficiency for incident angles that subtend spacecraft components prior to detection, and the efficiency map traces out the major spacecraft components surrounding the GRS; for example, the adapter ring and sunshade are clearly observed.

A4. Experimentally Measured Efficiency

[53] Sufficient data exist within the GRS data set to plot the background- and altitude-corrected 1779-keV Si gamma-ray count rates as a function of θ_n. The 1779-keV line was used in the place of the 1461-keV line because of the observation that its count rate does not vary substantially over the surface (Figures 5a, 6a, 6b, and 7a). Unlike the ground-calibration experiments and Geant4 simulations,